Princetonlaan 6
3584 CB Utrecht
P.O. Box 80015
3508 TA Utrecht
The Netherlands

www.tno.nl

T +31 88 866 42 56
F +31 88 866 44 75

TNO report

TNO2022_R11962

The PySub Subsidence Model Framework: Technical Reference

Date 14 maart 2023

Author(s)

Copy no
No. of copies
Number of pages 33 (incl. appendices)
Number of appendices 1
Sponsor Ministry of Economic Affairs and Climate Policy
Project name KEM-16
Project number 060.51941/01.06.07

Contents

1 Introduction

The PySub modelling framework contains tools to predict subsidence caused by mining activities and can make subsidence prognoses, show the results and statistical characteristics (uncertainty, maximum, etc.). This framework was developed by TNO-AGE by request of the KEM (Knowledge Programme on Effects of Mining)-programme. It has been developed in Python. The code repository is available on Github (https://github.com/TNO/PySub).

Subsidence is the vertical downward movement of the Earth's ground surface. Subsidence can occur naturally, but it also be (partially or completely) human induced.

The different causes of subsidence can work at varying timescales and occur at different depths in the subsurface. In many cases, natural large scale and deep causes such as tectonic and magmatic processes can be discarded compared to other natural and human induced subsidence. The rate at which subsidence at such large scale occurs is very low and the subsidence is uniform over large areas, causing little effect to structures. Natural causes of shallow subsidence include compaction of shallow soil due to peat oxidation or drainage of clay layers, sinkhole formation, and erosion. Subsidence can also be induced by mining activities, where resources such as water, hydrocarbons or salt are extracted from the subsurface.

The different types of mining-induced subsidence are distinguished by the phase of the extracted resource: gas or liquid phase, and solid phase. Gases or fluids can be present in the pore spaces of a porous rock (the reservoir). Extraction leads to a change in pore pressure that may cause compaction of the reservoir. The compaction is expressed as a volume change that causes the subsidence at the surface level (Figure 1-1).

In case of removing solid materials such as salt, the resulting cavern may change its shape due to the difference in lithostatic pressure and the pressure inside the cavern (Figure 1-2). In other words, the cavern is squeezed. The squeezing causes a change in shape and volume. This specific type of volume change is called the squeeze volume.

The location from where material (gas, liquid or solid phase) is mined is called a reservoir.

The PySub modelling framework was made with Dutch mining activities in mind. This primarily concerns the extraction of natural gas from the deep subsurface (generally between two to three km depth) and extraction of salt (generally from 500 to 2000 km depth). It should be noted that the vertical surface movement due to addition of material to a reservoir (storage) can also be determined with this framework.

The documentation of PySub is divided into four parts, including this document. The other parts are:

- The User Manuals: explaining how to fill the different templates

- Case study (TNO, 2023): as proof of concept, validation and showcase of PySub's functions and options to visualize the results.
- Code documentation (https://github.com/TNO/PySub): Where the code's modules, functions, classes and other data structures are explained. This also includes tutorials on working with PySub in Python code.

In this report we discuss the underlying methods used to calculate subsidence in PySub, as well as the methods of the technical pre- and processing tools.

The functionality of the framework can be separated into pre-processing, the calculations and the post-processing. In the pre-processing the user input is interpreted and converted into the required format for the calculation step (in case the interpretation or conversion step fail, an error or warning is returned). The post-processing allows for interpretation and clear visualisation of the results.

In the next chapter, Chapter 2, the general approach for calculating subsidence is discussed. Chapter 3 describes the methods to determine reservoir compaction caused by production of a gas or liquid. Chapter 4 treats the interpretation of the squeeze volume. In Chapter 5 different options for the influence functions are discussed. These functions determine subsidence from the volume changes. Additional functionalities for pre-processing and the statistical analysis of model results are treated in Chapter 6. Postprocessing and visualization options are described in more detail in the report discussing practical examples: the Case Study document (TNO, 2023). For manuals on how to use PySub we refer to the PySub User Manuals.

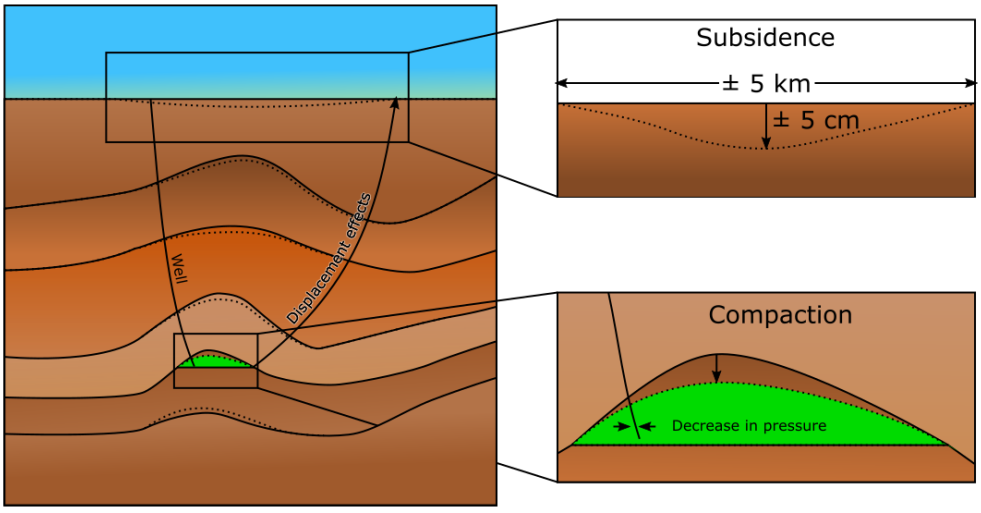

Figure 1-1 Graphical representation of subsidence due to pressure change in a reservoir.

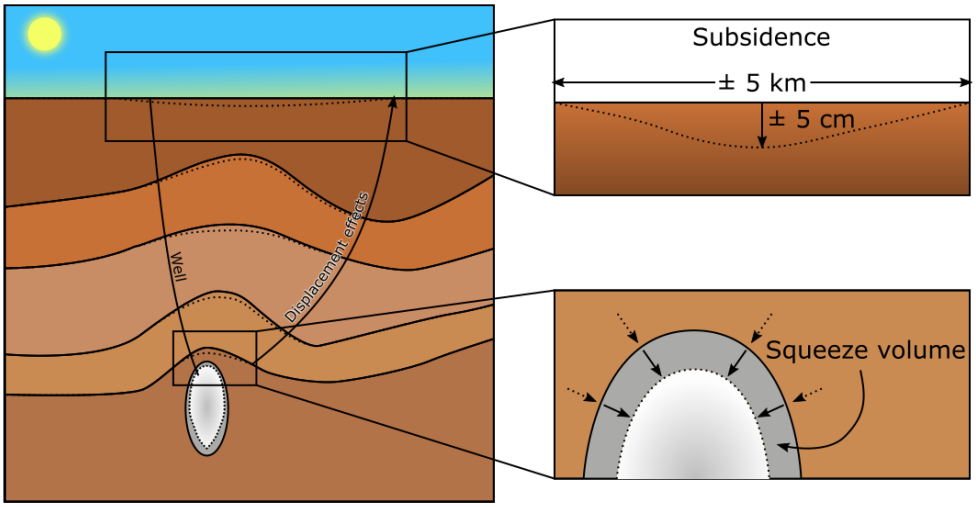

Figure 1-2 Graphical representation of subsidence due to the deformation of a cavern.

2 Model approach

This chapter discusses the subsidence calculation method. It describes how the input is represented in the model and the steps taken to make the subsidence predictions.

The model input depends on the method of compaction or the use of squeeze volume, and the choice of influence function (see Chapter 3 and 4 for more in-depth information). The definition of the variables are discussed in the user manual, including a list of required variables for the different methods.

2.1 Data architecture

The input is converted and the resulting information is stored in a uniformly spaced 2-dimensional grid (Figure 2-1), representing a virtual model of the studied area. The grid nodes are at locations within the studied area. Each grid node has reservoir parameters attached to them. Reservoir parameters include geomechanical properties, spatial information (e.g. depth) and the pressure development over time. Note that the stacked layers in Figure 2-1 are the reservoirs, not a representation of depth. The depth is stored as one of the parameters on a grid node.

The grid extent is based on the extent of the reservoir and the user-defined variables: influence radius and grid cell size. The model has the extent of all the defined reservoirs combined plus a buffer: the influence radius. The influence radius is the horizontal distance from a reservoir border at which the subsidence is considered to be negligible. A different model extent can also be specified manually.

The PySub framework has functionality to load grids and point clouds or unstructured grids storing information on spatially varying parameters. Because point clouds or unstructured grids do not necessarily have their values in a structured grid, bi-linear interpolation is used to convert the data into the required grid format. When uniform grids are used, they are forced to be linearly interpolated to the model grid to ensure that uniform input grids with different cell sizes and/or extents can be used.

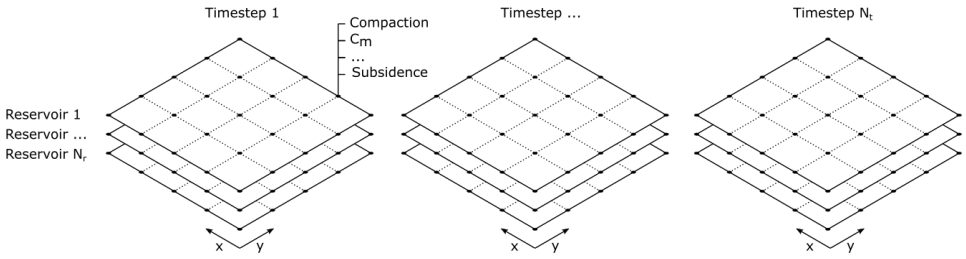

Figure 2-1 Visualisation of the model grid.

2.2 Calculation method

When the grid is initiated, it only stores the coordinates. After initialisation, four processing and calculation steps are followed:

First, grid nodes inside each reservoir are tagged using a mask: nodes inside the boundaries of a mining activity are tagged and those outside are not. Some mining activities are represented as points (locations of (salt) caverns). For each cavern point, only the nearest grid node is tagged.

Second, the volume change for each timestep is added as a variable to the grid nodes inside the reservoir by either setting it directly – in case a squeeze volume is given – or calculating the compaction based on the pressure profile from the input. The volume change is calculated for each grid node independently.

Third, the subsidence at the surface level is determined by applying influence functions. These influence functions describe the vertical displacement at the surface per unit of volume change at a grid node as a function of the horizontal and vertical distance from the volume change.

Each tagged grid node will induce subsidence at a distance much larger than the cell size each grid node represents. Therefore each (tagged and untagged) grid node can be affected by multiple tagged grid nodes. As the influence functions assume homogeneous linear (poro-)elastic behaviour of the subsurface. This allows for superposition of the effects of volume change (Figure 2-2).

NB: It should be noted that any non-linear processes due to viscous behaviour of salt on subsidence is not taken into account and beyond the scope of the model framework. The resulting subsidence is therefore a first-order indication of the subsidence in any case where mining occurs in or under salt formations.

Then, as a final fourth step, a combined influence function is calculated by summation of the individual influence functions in each reservoir over the spatial plane. Optionally (usually during the visualization process), the resulting subsidence of each reservoir is summed to display the total subsidence bowl or determine the maximum subsidence.

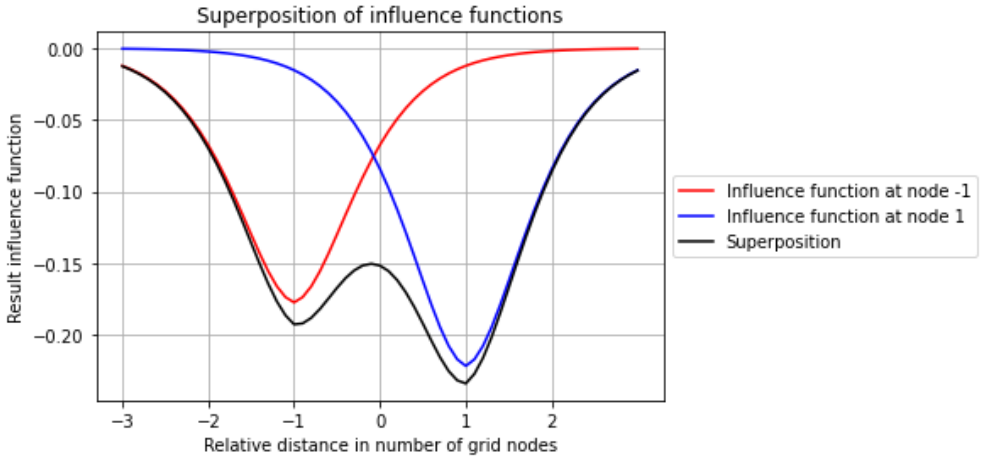

Figure 2-2 Visualisation of the results of a fictional influence function over 2 nodes at relative positions -1 and 1.

The model approach is shown stepwise in Box 1. The boxes are used to show more technical information.

Box 1 – Pseudocode of model workflow

The information is stored in a grid over spatial dimensions (over the x- and y-coordinate axes) and separately for each reservoir and timestep. The subsidence can be superimposed over all or selected reservoirs, due to the assumption of linearity of the subsidence processes.

A step-wise general implementation of the method to calculate subsidence is given here:

1. Pick an influence function $f(r)$, where *r* is the distance from the volume change, (see chapter 5) to determine the vertical ground displacement at each grid node *i*, per unit of volume change ($\frac{\Delta u_i}{\Delta V}$) using $\frac{\Delta u_i}{\Delta V} = f(r)$.
2. For each reservoir, perform steps 3 and 4:
    3. Tag the grid nodes inside the reservoir
    4. For each timestep, perform steps 5 and 6:
        5. Initiate the variables volume change (ΔV_i) and vertical ground surface motion (u_i) as 0 for each grid node *i*
        6. For each grid node *i* perform step 7:
            7. For each grid node *j* inside the reservoir, perform steps 8 to 11:
                a. If the pressure change is known:
                    8. Calculate ΔV_j as compaction (see chapter 3) using pressure change
                b. If the squeeze volume is known:
                    8. Add squeeze volume (see chapter 4) to ΔV_j
            9. Calculate $\frac{\Delta u_i}{\Delta V}_j$ using the chosen influence function (see chapter 5) and the distance between *i* and *j*
            10. Calculate the vertical ground surface motion at *i* caused by ΔV_j (u_{ij}) using $u_{ij} = \Delta V_j \frac{\Delta u_i}{\Delta V}_j$
            11. Apply superposition by adding u_{ij} to u_i

Notably, step 9, 10 and 11 describe convolution of an influence function kernel over a 2D distribution of volume change.

3 Compaction

Pressure reduction due to extraction of liquids or gasses from a reservoir may lead to compaction in the reservoir and associated subsidence (e.g. Fjaer et al., 2008; Jaeger et al 2007). For PySub we assumed that all pressure changes will lead to compaction and that all reservoir compaction will cause subsidence.

The pressure development over time can be entered into the model to calculate the resulting compaction. The models that are used to calculate the compaction in the reservoir are: the linear and time-decay models and a stress rate dependent compaction model. The different models, their uses, limitations and methods are described below.

3.1 Linear compaction model

The linear compaction model (e.g. Fjaer et al. 2008, Jaeger et al. 2007) is a time-independent elastic model which determines the vertical strain based on the pressure depletion and compaction coefficient (c_m). Multiplying the vertical strain with the volume (V) of the grid cell, gives the amount of compaction in that grid cell. The linear compaction model determines the compaction at steady state, so any rate or time-dependent behaviour is not taken into consideration.

Equation 3-1:

$$\Delta V = V c_m (P_0 - P)$$

Where P is the pressure at the requested timestep and P_0 the comparative pressure.

3.2 Time-decay compaction model

One of the time dependencies observed during the study of subsidence time series is a delay in subsidence. This delay can be modelled using the time-decay compaction model (Mossop, 2012). The time-decay compaction model uses an exponential decay function with the time parameter τ. This parameter is a factor of time and determines the delay in compaction.

The parameter τ is often derived from observations by comparing the delay of observed subsidence to the relative pressure drop in the reservoir. When set to zero, this compaction model becomes the linear compaction model.

Box 2 – Time-decay formulation of compaction

The time decay function is a function for determining compaction which is not derived from any physical processes describing that process. It is a general function where the effects of a step function are delayed by a factor of **T** over time (t).

Equation 3-2:

$$\boldsymbol{T}(\Delta t, \tau) = \begin{cases} 1 - exp\left(\frac{-\Delta t}{\tau}\right) & : \Delta t \geq 0 \\ 0 & : \Delta t < 0 \end{cases}$$

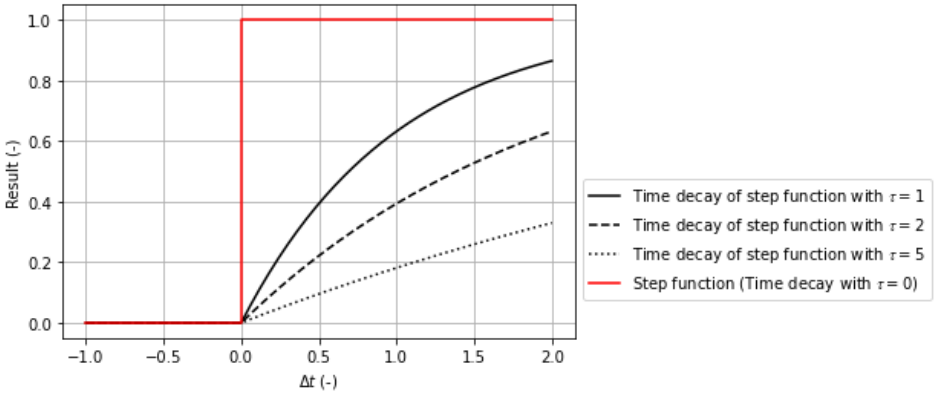

Figure 3-1 Time decay of step function for tau = [1, 2, 5].

Equation 3-3:

$$\Delta V(t) = V c_m (P_0 - P) * \boldsymbol{T}(\Delta t, \tau)$$

Because the pressure at different timesteps can change, the effect of any pressure change from previous timesteps should be taken into consideration using temporal superposition. Therefore:

Equation 3-4:

$$\Delta V = V\, c_m \sum_{j=1}^{i} \left(P_{j-1} - P_j\right) * \boldsymbol{T}\left(t_i - t_j, \tau\right) \qquad : i = (1 \ldots N)$$

Where P and t are 1-dimensional vectors with the length of the number of timesteps (N). The subscripts of P and t indicate the corresponding timestep of the these variables. A visual approach of Equation 3-4 is given in Figure 3-2.

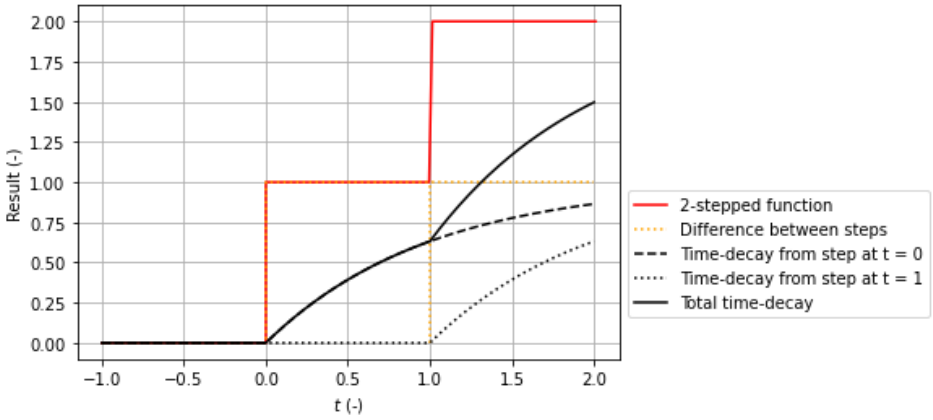

Figure 3-2 Time-decay (τ= 1) and temporal superposition.

3.3 Rate type compaction model

Another model developed to explain the observed delay in compaction is the rate type compaction model. This model explains this delay with a dependency on the rate of pressure change. The time-decay method is often used when only observations of subsidence are available, while the rate type compaction model can also incorporate data on geomechanical parameters. Geomechanical parameters are obtained from laboratory experiments where rock samples are tested under different stress and temperature conditions. The original rate type compaction model used an empirical model to simulate the rate-dependent behaviour (De Waal 1986). A limitation of this method is its inability to describe compaction during changing loading rates.

To make determining compaction with changing loading rates possible, this model has been expanded with the isotach formulation (Pruiksma et al., 2015). An isotach is a line describing the relationship between the stress and strain observed at constant stress rates. The relationship between stress and strain becomes linear at high enough stresses and below the yield point (e.g. Fjaer et al., 2008; Jaeger et al., 2007). In PySub, compaction is assumed to occur in the linear stress-strain domain.

With the isotach formulation, the rate type compaction model has unified the compaction behaviour with changing stresses and constant stresses. In the transition from a non-zero stress rate, to a constant stress, the description of creep at the constant stress phase is used to explain the delay in subsidence observed in laboratory and field observations (De Waal, 1986; Pruiksma et al., 2015; Van Thienen-Visser et al., 2012).

By setting the rate type compaction variable “reference stress rate” to 0, this method is equivalent to the linear compaction model.

Box 3 – Rate type compaction with isotach formulation

The rate type compaction model requires two parameters describing the initial state: reference stress (σ_{ref}) and reference stress rate ($\dot{\sigma_{ref}}$). Additionally it requires the constants: (direct) compaction coefficient ($c_{m,d}$), reference compaction coefficient ($c_{m,ref}$) and creep coefficient b. The reference stress rate can be determined using the local geological history and the reference stress can be determined with properties of the overburden.

The rate type compaction method with isotach formulation can be summarized as:

$$\varepsilon = \text{RTiCM}(P, \sigma_{ref}, \dot{\sigma_{ref}}, c_{m,d}, c_{m,ref})$$

1. Initialize the current shear and direct strain ($\varepsilon_{s,i=0}$ and $\varepsilon_{d,i=0}$) as 0 and calculate the necessary state parameters:

   $\varepsilon_{ref} = -c_{m,ref}\sigma_{ref}$
   $\sigma_{ref} = \rho g d_r$
   $\varepsilon_{i=0} = 0$

2. For every timestep i between 1 and N:
   $\sigma_i = \sigma_{ref} - P_i$
   $\dot{\varepsilon_s} = \left(\frac{\varepsilon_i - \varepsilon_{ref}}{\sigma_i}\right)\dot{\sigma_{ref}}\left(\frac{\varepsilon_i - \varepsilon_{ref}}{\sigma_i c_{m,ref}}\right)^{\frac{-1}{b}}$
   $\varepsilon_{s,i} = \varepsilon_{s,i-1} + \dot{\varepsilon_s}(t_i - t_{i-1})$
   $\varepsilon_{d,i} = c_{m,d}(\sigma_i - \sigma_{ref})$
   $\varepsilon_i = \varepsilon_{d,i} + \varepsilon_{s,i}$

The strain can be converted to volume change:

$$\Delta V = V\varepsilon$$

Where:

ε_i = total strain at timestep i
ρ = bulk density of the overburden in kg/m^3
g = gravitational acceleration of 9.81 m/s^2
d_r = depth of the reservoir top in m
$\dot{\varepsilon_{s,i}}$ = shear strain rate at timestep i

When there is too much time between the different timesteps ($t_i - t_{i-1}$), ε_s might be overestimated because $\dot{\varepsilon_s}$ registers a large difference between the current strain and reference strain ($\varepsilon_i - \varepsilon_{ref}$). Interpolation of P over time might be required to negate this numerical issue by increasing the number of timesteps and decreasing $t_i - t_{i-1}$. The degree of interpolation ($\boldsymbol{I}$, which here means interpolate at every $2^{\boldsymbol{I}}$ between known points) is estimated by the PySub framework using multiple solutions with increasing degrees of interpolation and taking the difference between the previous solution until convergence ($\epsilon = 2.5 * 10^{-6}$):

Initiate:

$\Delta = \infty$
$\boldsymbol{I} = 0$
$\varepsilon_{compare} = RTiCM\left(P, \sigma_{ref}, \dot{\sigma_{ref}}, c_{m,d}, c_{m,ref}\right)_{\boldsymbol{I}}$

While $\Delta < \epsilon$:

$\boldsymbol{I} = \boldsymbol{I} + 1$
$\varepsilon = RTiCM\left(P, \sigma_{ref}, \dot{\sigma_{ref}}, c_{m,d}, c_{m,ref}\right)_{\boldsymbol{I}}$
$\Delta = max\left(\left|\varepsilon_{compare} - \varepsilon\right|\right)$
$\varepsilon_{compare} = \varepsilon$

4 Squeeze volume

When the volume of any cavern changes, this volume change can cause subsidence. It must be noted that the volume change mentioned here does not mean the removal of material, but the changing of shape due to pressure differences in- and outside the cavern. This volume change is called the squeeze volume. PySub calculates the subsidence caused by this volume change by squeezing using the influence functions described in Chapter 5.

The squeeze volume of the cavern over time is dependent on many factors and is not a result of input parameters of PySub. This squeeze volume is required as input when calculating the subsequent subsidence.

Because the squeeze volume change of the cavern is used as an input variable, subsidence due to more complex histories of cavern volumes development can be determined. One of these processes is the production of salt, which due to the viscous behaviour of the material has a non-linear shut-in profile over time. A non-linear shut-in profile means that the rate of volume change of the cavern is not constant.

4.1 Salt caverns

An occurrence of squeeze volume can be caused by any process resulting in a pressure difference between a cavern and the material outside the cavern. In the Netherlands the most predominant process that causes this, is salt mining. By injecting sweet water in salt bearing rock, the salt is dissolved and the resulting brine is transported to the surface. The pressure difference between the inside of the salt-cavern and the surrounding salt causes squeeze volume. Assumptions and considerations when using this model for subsidence caused by salt mining is discussed here as well.

4.2 Vertical extent

The volume change entered in the model is the amount of squeeze volume that occurs in each timestep and will be distributed uniformly over the entire cavern.

Generally, caverns do not have a large extent in the horizontal plane, and the PySub model therefore only takes x- and y-coordinates of the cavern centre(s). To take into account elongated shapes (or flatter, “pancake”-like shapes), a length is also requested. This length represents the vertical extent of the cavern. The elongated shape of caverns is taken into account by stacking grid cells and weighing their contributions to the influence function with the volume V in m^3.

In Figure 4-1, the representation of an elongated cavern is shown. The cavern length is 3.5 times the horizontal grid-space (Δx). Which is $7/8^{th}$ of the representation in grid units. The squeeze volume change is then distributed over 4 grid cells. Instead of uniformly (with $1/4^{th}$ of the squeeze volume change in each cell), the distribution follows the length of the cavern present in each grid cell. In our

example of Figure 4-1, each of the top 3 cells will have 2/7th's of the total squeeze volume change of the cavern and the bottom cell 1/7th.

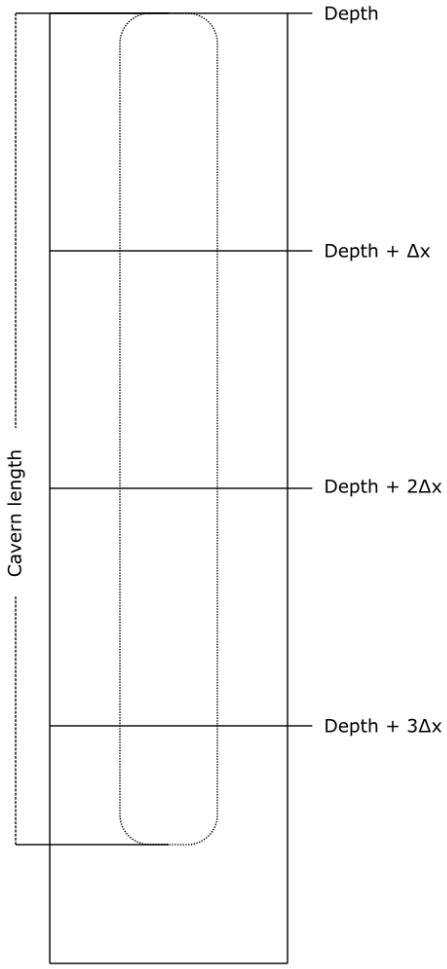

Figure 4-1 Representation of elongated cavern in grid.

5 Influence functions

The influence functions in this report describe the vertical displacement at the surface as a function of the distance to a point source, and the volume change at that point source. Three different analytical influence functions are available within the PySub Framework: Geertsma, Van Opstal and Knothe. All three functions require a volume change in the subsurface to determine the subsidence. Below, the methods of each function are discussed.

5.1 Nucleus of strain

In 1973 Geertsma published an analytical poro-elastic influence function for determining subsidence from compaction in a reservoir. The reservoir is assumed to be surrounded by an infinite medium with constant elastic properties. The overburden is represented by a semi-infinite half-space. This half-space has a surface, but an infinite depth below the reservoir. The reservoir is represented as a point, or nucleus, on a grid node where the volume change or strain occurs. By using multiple nuclei it is possible to determine the subsidence (u^*) due to compaction in complex reservoir shapes.

The method requires the following input parameters: the depth of the reservoir ($\mathrm{d_r}$), the horizontal distance from the nucleus (r), and the Poisson's ratio (ν) of the bulk rock.

In 1974 this method was expanded on by Van Opstal, who added a correction (u^*) for a perfectly rigid basement at a finite distance below the reservoir. This solution shows less subsidence at the deepest point of the subsidence bowl and a smaller subsidence bowl compared to the Geertsma solution. Unlike the Geerstma method, the Van Opstal method results in a subsidence bowl with a volume equal to that of the compaction volume. At the peripheries of the subsidence bowl, uplift might occur, but this uplift is orders of magnitude smaller than the subsidence.

The subsidence bowl shape and maximum subsidence obtained with the Van Opstal method fit better with the observations (e.g. Van Thienen-Visser et al., 2015).

The Van Opstal solution has as an additional input: the depth to the rigid basement (d_b). This parameter has an influence on the depth of the deepest point in the subsidence bowl and the shape of the subsidence bowl.

5.2 Knothe

The Knothe model uses a gaussian distribution to calculate subsidence and is based on the depth of the reservoir and the influence angle of the reservoir. This method is mainly used in extraction mining, where for instance coal is removed from coal seams (Sroka, 2011).

The influence angle of the subsidence bowl determines the shape of the modelled subsidence bowl and can be determined by fitting observations to the result of this function.

The difference between the maximum subsidence calculated by the Knothe influence function and the nucleus of strain method is dependent on the chosen variable determining the shape of the subsidence bowl. This variable is the influence angle for the Knothe method and the depth to the rigid basement for the nucleus of strain method. If both models yield the same subsidence at the deepest point of the subsidence bowl, the shape of the subsidence bowl between the two methods is slightly different (Figure 5-1), which is most apparent at the flanks of the subsidence bowl (Van Thienen-Visser et al., 2016).

Box 4 – Influence functions

Influence functions describe the vertical displacement that a volume change at a point source has on a point at a specified distance and can be described as:

$$\frac{\Delta u}{\Delta V} = f(r, \ldots)$$

Where f is the influence function and r the distance from the point of volume change. In this box the formulas of the above mentioned influence functions are shown and a comparison is made visual in Figure 5-1.

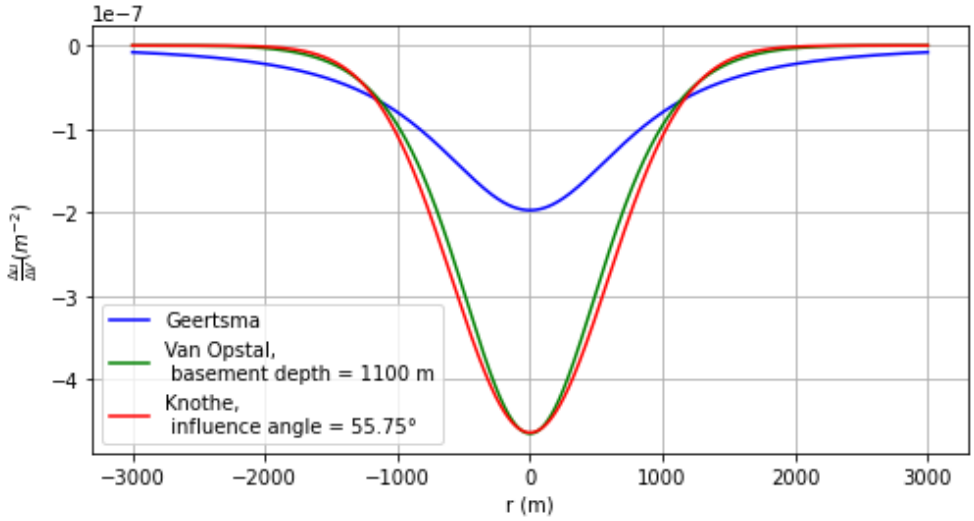

Figure 5-1 The 3 discussed influence functions compared with standardised parameters (Poisson's ratio (ν) = 0.25, d_r = 1000 m, additional parameters in legend).

Geertsma:

$$f_{Geertsma}(r, d_r) = \frac{1-\nu}{\pi} \frac{d_r}{r^2+d_r^2}$$

Van Opstal:

$$f_{Van\ Opstal}(r, d_r, d_b, \nu) = f_{Geertsma}(r, d_r) + u^*(r, d_r, d_b, \nu)$$

Where:

$$u^*(r, d_r, d_b, \mathrm{I}, \mathrm{J}, a_{1i}, a_{2i}, b_{1j}, b_{2j}) = \frac{1-\nu}{2\pi}\left(\sum_{i=1}^{I} \alpha_i(r, d_r, d_b, a_{1i}, a_{2i}) + \sum_{j=1}^{J} \beta_j\left(r, d_r, d_b, b_{1j}, b_{2j}\right)\right)$$

The functions α and β are polynomials dependent on parameters $I, J, a_{1i}, a_{2i}, b_{1j}$ and b_{2j} and are further expanded on in Appendix A. These functions can be repeated and summed to achieve higher accuracy. For I = 2 and J = 1 the accuracy of the approximation is considered sufficient (Van Opstal, 1974). The variables a_{1i}, a_{2i}, b_{1j} and b_{2j} are to be adjusted for different Poisson ratios. Van Opstal has only presented the approximation for a Poisson ratio of 0.25, representative for average sedimentary rocks (Van Opstal, 1974). For PySub, novel analytical approximations of a_{1i}, a_{2i}, b_{1j} and b_{2j} for other Poisson's ratios were constructed. These are described in Appendix A.

Box 4 continues on the next page.

Box 4 – Continued

Knothe:

$$u = \frac{1}{R^2} exp\left(\frac{-\pi r^2}{R^2}\right)$$

Where R is dependent on the influence angle φ in degrees:

$$R = d_r \, \pi \, tan(\varphi/180)$$

6 Additional tools

To perform the subsidence calculations with PySub, specific types of data are needed, and in specific formats (See User Manuals). In some cases this data is not available as required. To convert that data, pre-processing tools are built in. The following pre-processing features are available in the framework and described here:

- Conversion from virgin pressure and end pressure to pressure profile

Post-processing features include the creation of figures (described in TNO, 2023), but also statistical methods to indicate uncertainty in the model results. In PySub the following statistical methods are implemented and discussed here:

- Ensemble methods
    - Bucket ensemble

6.1 Virgin pressure and end pressure to pressure profile

The pressure profile (pressure over time), needed to predict the compaction, can be determined using observations or reservoir models. When the pressure profile of the reservoir is known, it is recommended to use this as input to the PySub model. However, the complete profile is often not available in the public domain. Therefore, an additional functionality automatically converts the initial and abandonment pressure to a pressure profile. Observations and model predictions have been normalized on both pressure difference and time and compiled into a dataset. When only the start- and end time and the start- and end pressure are entered, the normalized pressure timeseries, are re-projected from these values. The reprojected pressure-time curves are a first-order estimate of a realistic pressure profile for fields that have limited predictions of their pressure profile.

In Figure 6-1, normalized curves of pressure development over time of 4 different gas fields are shown that describe the shape of the pressure decline over time. The different curves represent different production duration scenarios. The pressure difference also is different between scenarios, but normalized in the figure.

For a short production duration the pressure profile is almost linear, while the pressure profile becomes more convex for longer durations. The difference between the normalized profile of the 10-year scenario and the 47- year scenario have a certain deviation. Here, this deviation is deemed small enough to be considered constant for a first-order estimate of the pressure profile. In the PySub framework, a reservoir that is producing for longer than 10 years will therefore have a constant normalized pressure profile.

Only reservoirs that do not have a complex pressure history have been selected for the dataset. Other situations that can cause more complex pressure profiles include:

- Difference in timing of production
- Neighboring reservoir compartments influencing the reservoir pressure.

The pressure profile is therefore only representative for a relatively simple pressure development in the reservoir(s).

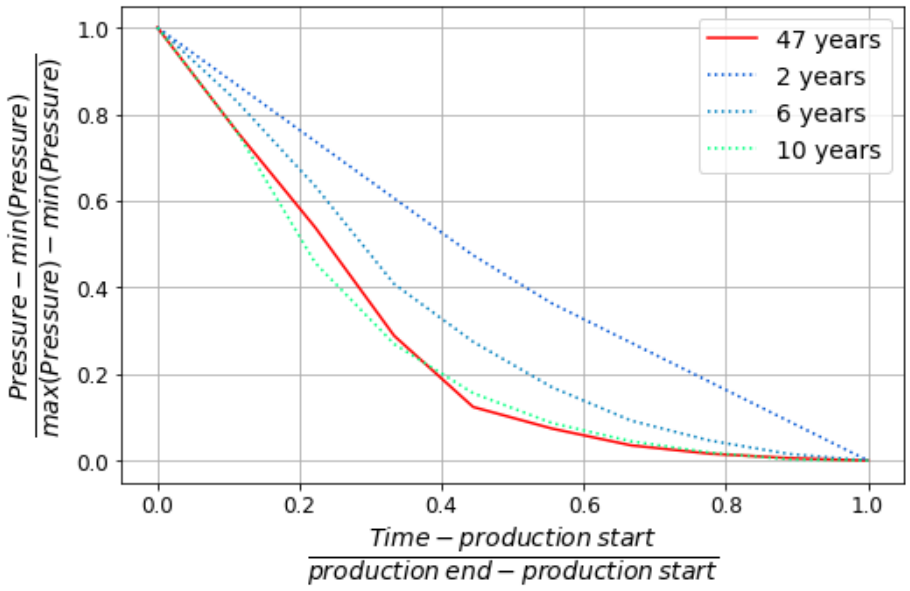

Figure 6-1 Normalized pressure curves of the modelled reservoir pressure from the observed pressures of the gas field Annerveen in the Netherlands (solid line) and pressure predictions for the gas field Leemdijk (dotted lines; Vermillion Energy Netherlands B.V., 2020).

6.2 Ensemble methods

Ensemble methods run multiple models with randomly sampled or deterministic parameters to construct a distribution of the possible results. These distributions can subsequently be used to determine the likelihood of a specific result. When the input parameters of a model are given a probability of occurrence, by either assigning probabilities for specific values or a probability distribution, a probability of the result can be obtained.

A result of one such ensemble is shown in Figure 6-2. On the x-axis, the displayed curve shows the result for the maximum subsidence in each realization. The realizations are sorted in ascending order of the maximum subsidence in their subsidence bowl. The y-axis shows the cumulative probability of each realization occurring. The resulting distribution allows the user to visualize the probability of a specified maximum amount of subsidence to occur.

When considering worst-case scenarios, the P90 value of subsidence is often used. This value is the subsidence at which only 10% of the values are exceeding that subsidence magnitude. In the case of Figure 6-2 the P90 subsidence is 4.12 cm. The P50 value can therefore be considered the median (the mean if the probability distribution is a normal distribution).

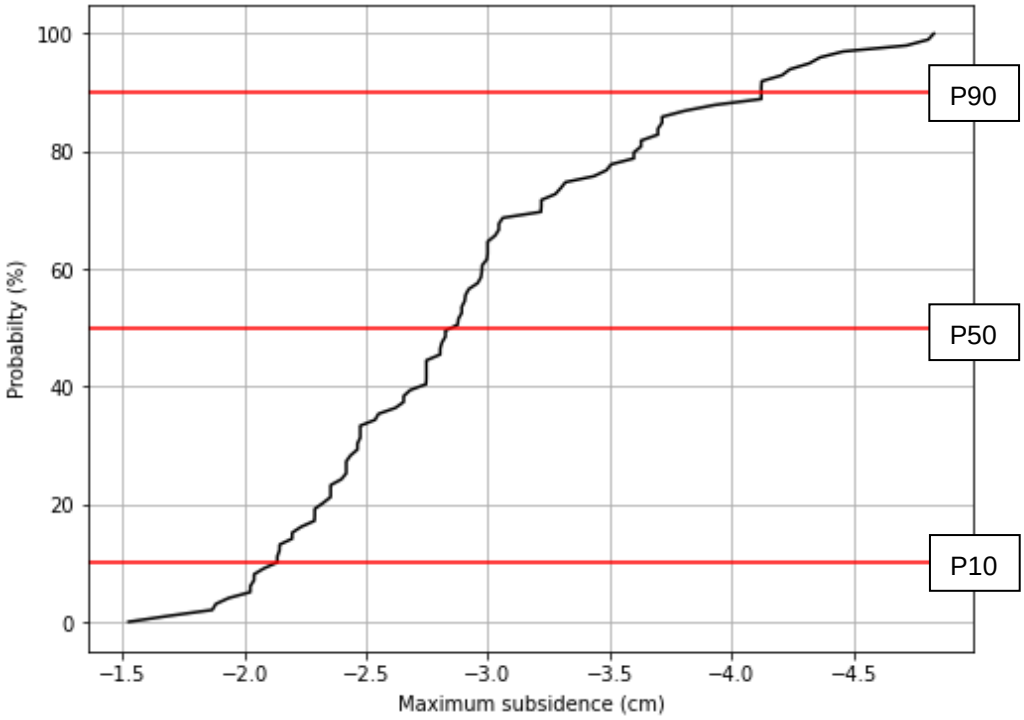

Figure 6-2 Probability distribution of the maximum subsidence as a result of a 100 member ensemble sampler for a fictional gas reservoir. Note that the stepped curve shape is caused by a limited number of ensemble members in combination with the sampling from discrete values (instead of a distribution) as part of the ensemble method used : the Bucket Ensemble method.

The model results of each run can be compared to observations. The realization with results that show the least deviation, can be considered a best fit. The parameters that served as input to this model realization can be considered a first-order estimate of the relevant physical parameters.

The ensemble method currently implemented in PySub (the Bucket ensemble method) is described in the next section.

6.2.1 Bucket ensemble

The bucket ensemble method uses fixed specified values with a corresponding probability. For instance, in Table 6-1, the reservoir thickness is defined as 3 discrete values and with corresponding probabilities.

Table 6-1 Example input

Version	**Reservoir thickness (m)**	**Probability (ratio)**
Minimum	25	0.3
Medium	50	0.5
Large	75	0.2

When the ensemble samples for values, it selects from one of these discrete values. Instead of sampling from a continuum, the ensemble samples from a finite amount of “Buckets” with the assigned probability. The probability of the ensemble

selecting the minimum scenario is 0.3 (or 30%). The probabilities of each parameter must add up to 1.

Besides the method where random samples are drawn, there is also a deterministic method available for the bucket ensembles. All possible combinations are determined and their results stored. Each realization has a probability of occurrence based on the product of all its parameter probabilities. The sum of all possible combination probabilities is 1. This means that a similar distribution to Figure 6-2 can be made and the P10, P50 and P90 can be determined.

7 References

Fjaer E, Holt RM, Horsrud P, Raaen AM (2008). Petroleum related rock mechanics. *Elsevier*.

Fokker PA, Osinga S (2018) On the use of influence functions for subsidence evaluation, American rock mechanic's association, 52nd US Rock Mechanics/Geomechanics Symposium.

Geertsma J (1973) Problems of rock mechanics in petroleum engineering. Proc. First Congr. Of the Int. Soc. Of Rock Mech., 1, 585.

Jaeger JC, Cook NGW, Zimmerman RW (2007) Fundamentals of Rock Mechanics 4th edition, Oxford, UK: Wiley-Blackwell.

Mossop A (2012) An explanation for anomalous time dependent subsidence, 46th US Rock Mechanics/Geomechanics Symposium, Chicago, Illinois, USA, 24–27 June 2012, 12-518.

Van Opstal GHC (1974) The effect of base-rock rigidity due to reservoir compaction, Adv, in Rock Mech., 3, 1103-1111.

Pruiksma J, Breunese JN, Thienen-Visser K, De Waal JA (2015) Isotach formulation of the Rate Type Compaction Model for sandstone, Int. J. Rock Mech., 78, 127–132.

Van Tienen-Visser K, Pruiksma JP, Breunese JN (2015) Compaction and subsidence of the Groningen gas field in the Netherlands, Proceedings of the International Association of Hydrological Sciences 372: 367-373.

Van Thienen-Visser K, Juez-Larré J, Remmelts G (2016) De prognose van bodemdaling en de kans op beven door gasproductie uit het Oppenhuizen gasveld. TNO-AGE 16-10.068.

De Waal J (1986) On the rate type compaction behaviour of sandstone reservoir rock, PhD thesis, Delft University of Technology, Delft, the Netherlands, available at: http://repository.tudelft.nl/view/ir/ uuid:b805782b-2eb4-4f72-98f4-f727c4ea9df0.

TNO (2023) Toolbox subsidence (KEM-16). Discriminating subsidence contributions from multiple mining activities; case study Diever, Vinkega and Eesveen area, TNO report: TNO2022_R11963.

Sharma B (1956) Stresses in an infinite slab due to a nucleus of thermo-elastic strain in it, Journal of applied mathematics and mechanics 35: 926-930.

Sroka A, Tajdus K, Preusse A (2011) Calculation of Subsidence for Room and Pillar and Longwall Panels, Proceedings of the 2011 Coal Operators' Conference, Mining Engineering, University of Wollongong, 18-20 February 2019.

Vermillion Energy Netherlands B.V. (2020) Winningsplan Leemdijk-De Bree-Smitstede. https://www.nlog.nl/kaart-boringen

8 Signature

Utrecht, 14-03-2023

J.H.J Ebbing
Acting Head of department

A Terms of the α- and β-series

In Chapter 5.1, the Van Opstal method to determine subsidence is discussed. The formula for u^* contains the polynomials α and β. These polynomials are expanded on, here (Van Opstal, 1974).

The α series is defined as:

$$\alpha = \sum_{m=1}^{7} \frac{\mathrm{f}_m(d_r, d_b, \nu, a_{1i}, a_{2i})}{(r^2 + g_m(d_r, d_b, a_{2i})^2)^{\frac{n_m}{2}}}$$

Where f_m and g_m are polynomials that take different shapes for m and $\mathrm{n_m}$ takes values of 3, 5 and 7 only. The complete formulation is shown here:

$$\alpha = \frac{a_{1i}(a_{2i}d_b - d_r) - 2a_{1i}d_b}{(r^2 + (a_{2i}d_b - d_r)^2)^{\frac{3}{2}}}$$

$$+\frac{2a_{1i}d_b - (3-4\nu)^2 a_{1i}(a_{2i}d_b + d_r)}{(r^2 + (a_{2i}d_b + d_r)^2)^{\frac{3}{2}}}$$

$$-\frac{(3-4\nu)a_{1i}(a_{2i}d_b + 2d_b + d_r)}{(r^2 + (a_{2i}d_b + 2d_b + d_r)^2)^{\frac{3}{2}}}$$

$$+\frac{(3-4\nu)a_{1i}(a_{2i}d_b + 2d_b - d_r)}{(r^2 + (a_{2i}d_b + 2d_b - d_r)^2)^{\frac{3}{2}}}$$

$$-\frac{6a_{1i}d_b(a_{2i}d_b - d_r)^2}{(r^2 + (a_{2i}d_b - d_r)^2)^{\frac{5}{2}}}$$

$$+\frac{6a_{1i}d_b(a_{2i}d_b + d_r)\big(6d_b - (a_{2i}d_b + d_r)\big)}{(r^2 + (a_{2i}d_b + d_r)^2)^{\frac{5}{2}}}$$

$$-\frac{60a_{1i}d_b^2(a_{2i}d_b + d_r)^3}{(r^2 + (a_{2i}d_b + d_r)^2)^{\frac{7}{2}}}$$

The β-series is defined as:

$$\beta = \sum_{k=1}^{11} \frac{\mathrm{f}_k(d_r, d_b, \nu, b_{1i}, b_{2i})}{(r^2 + g_k(d_r, d_b, b_{2i})^2)^{\frac{n_k}{2}}}$$

Where f_k and g_k are polynomials that take different shapes for k and n_k takes values of 3, 5, 7 and 9 only. The complete formulation is shown here:

$$\beta = -\frac{b_{1j}d_b}{\left(r^2+\left(b_{2j}d_b-d_r\right)^2\right)^{\frac{3}{2}}}$$

$$+\frac{(3-4\nu)^2 b_{1j}d_b}{\left(r^2+\left(b_{2j}d_b+d_r\right)^2\right)^{\frac{3}{2}}}$$

$$-\frac{(3-4\nu)b_{1j}d_b}{\left(r^2+\left(b_{2j}d_b+2d_b-d_r\right)^2\right)^{\frac{3}{2}}}$$

$$+\frac{(3-4\nu)b_{1j}d_b}{\left(r^2+\left(b_{2j}d_b+2d_b+d_r\right)^2\right)^{\frac{3}{2}}}$$

$$-\frac{3b_{1j}d_b\left(b_{2j}d_b-d_r\right)\left(6d_b-\left(b_{2j}d_b-d_r\right)\right)}{\left(r^2+\left(b_{2j}d_b\ -\ d_r\right)^2\right)^{\frac{5}{2}}}$$

$$+\frac{3b_{1j}d_b\left(b_{2j}d_b+d_r\right)\left(6d_b-(3-4\nu)^2\left(b_{2j}d_b-d_r\right)\right)-36b_{1j}d_b^3}{\left(r^2+\left(b_{2j}d_b+d_r\right)^2\right)^{\frac{5}{2}}}$$

$$+\frac{3(3-4\nu)b_{1j}d_b\left(b_{2j}d_b+2d_b\ -\ d_r\right)^2}{\left(r^2+\left(b_{2j}d_b+2d_b\ -\ d_r\right)^2\right)^{\frac{5}{2}}}$$

$$-\frac{3(3-4\nu)b_{1j}d_b\left(b_{2j}d_b+2d_b+d_r\right)^2}{\left(r^2+\left(b_{2j}d_b+2d_b+d_r\right)^2\right)^{\frac{5}{2}}}$$

$$+\frac{30b_{1j}d_k^2\left(b_{2j}d_b-d_r\right)^3}{\left(r^2+\left(b_{2j}d_b-d_r\right)^2\right)^{\frac{7}{2}}}$$

$$+\frac{30b_{1j}d_k^2\left(b_{2j}d_b+d_r\right)^2\left(12d_b-\left(b_{2j}d_b+d_r\right)\right)}{\left(r^2+\left(b_{2j}d_b+d_r\right)^2\right)^{\frac{7}{2}}}$$

$$+\frac{420b_{1j}d_k^3\left(b_{2j}d_b+d_r\right)^4}{\left(r^2+\left(b_{2j}d_b+d_r\right)^2\right)^{\frac{9}{2}}}$$

A.1 Approximating the terms of the α- and β-series

These polynomials are derived from the description of elastic strain given by Sharma (1956), which starts with the Hankel transform (at the free surface):

$$u^* = \frac{1-\nu}{2\pi\sqrt{r}}\int_0^\infty \lambda^{-\frac{1}{2}} C(\lambda) J_0(\lambda r) d\lambda$$

Where J_0 is a Bessel function of the first kind with order 0, λ is an unknown function representing the distance from the nucleus of strain in Hankel space.

$$C = \frac{\lambda}{2\phi}\left[e^{\lambda d_r}(2\lambda d_b + 1) - e^{-\lambda d_r}(4\lambda^2 d_b^2 + 2\lambda d_b + (3-4\nu)^2) - (3-4\nu)\left(e^{-\lambda(2d_b+d_r)} - e^{-\lambda(2d_b-d_r)}\right)\right]$$

and

$$\phi(\lambda d_b) = (1-2\nu)^2 + \lambda^2 d_b^2 + (3-4\nu)cosh^2(\lambda d_b).$$

Also described as:

$$\mathbf{\Phi} = 1/(2\phi)$$

Some functions have a known analytical solution of the Hankel transform. But due to the complex nature of the **Φ** function, this is not applicable. Therefore, the **Φ** function can be approximated with functions that do have a known solution of the Hankel transform. This function has been approximated using (Van Opstal 1974):

$$\mathbf{\Phi}_{\mathbf{VanOpstal}}(\lambda d_b, I, J, a_{1i}, a_{2i}, b_{1j}, b_{2j}) = \sum_{i=1}^{I}\left(a_{1i}e^{-a_{2i}\lambda d_b}\right) + \sum_{j=1}^{J}\left(b_{1j}\lambda d_b e^{-b_{2j}\lambda d_b}\right)$$

The solution of the Hankel transform has been given in the above α and β polynomials.

The a_{1i}, a_{2i} and b_{1j}, b_{2j} terms of the α- and β-series are dependent on the Poisson's ratio (ν). Van Opstal (1974) only defined the values of these terms for the Poisson's ratio 0.25. For other values of ν representative for elastic rock properties in the subsurface (0.1 to 0.35) these terms have not yet been defined. Here, the methods and results are discussed to determine these terms for different Poisson's ratios and the derivation of a function for each of these terms dependent only on the Poisson's ratio.

Firstly, one needs to solve the **Φ** function for different Poisson's ratios (0 to 0.45) and a realistic range of λd_b (here 0 to 10 is chosen). After this, every Poisson's ratio has a distribution dependent on λd_b through which the $\mathbf{\Phi}_{\mathbf{VanOpstal}}$ has been fitted through by iteratively choosing the set of terms that result in the lowest deviation from **Φ** (least square method). The resulting terms ($terms'$) are plotted in Figure A-1 (red markers).

Note:
The parameter a_{11} is set to 1 and then a_{12} can be determined by setting the λd_b values in **Φ** to 0 over different Poisson's ratios. The results can be described analytically by:

$$a_{12} = \frac{1}{8-16\nu+8\nu^2} - 1$$

Other terms are more challenging to determine analytically and therefore the least square method has been used once more to determine these terms. This also includes a polynomial approximation of the a_{12} term to allow for a better fit by compensating for the other terms.

For convenience and extra flexibility, a function has been fitted through these resulting terms using the least square method with the aim to create an analytical function that determines these terms for different Poisson's ratios ($F_{term}(0 < \nu < 0.45)$) such that:

$$term = F_{term}(\nu)$$

The general polynomial to fit through each function has been chosen to be the 10th order polynomial:

$$F_{term}(\nu) = \sum_{\omega=0}^{10} c_{\mathrm{term},\omega}\nu^{\omega}$$

Where $c_{term,\omega}$ is a constant for each term (a_{1i}, a_{2i} and b_{1j}, b_{2j}) and exponent (ω).

In Figure A-1 the results of $F_{term}(\nu)$ are shown together with the $term'$ in solutions and in Table A-1 the $c_{term,\omega}$ solutions are shown. Table A-2 shows the coefficients for Poisson's ratio 0.1 to 0.35 with an interval of 0.05.

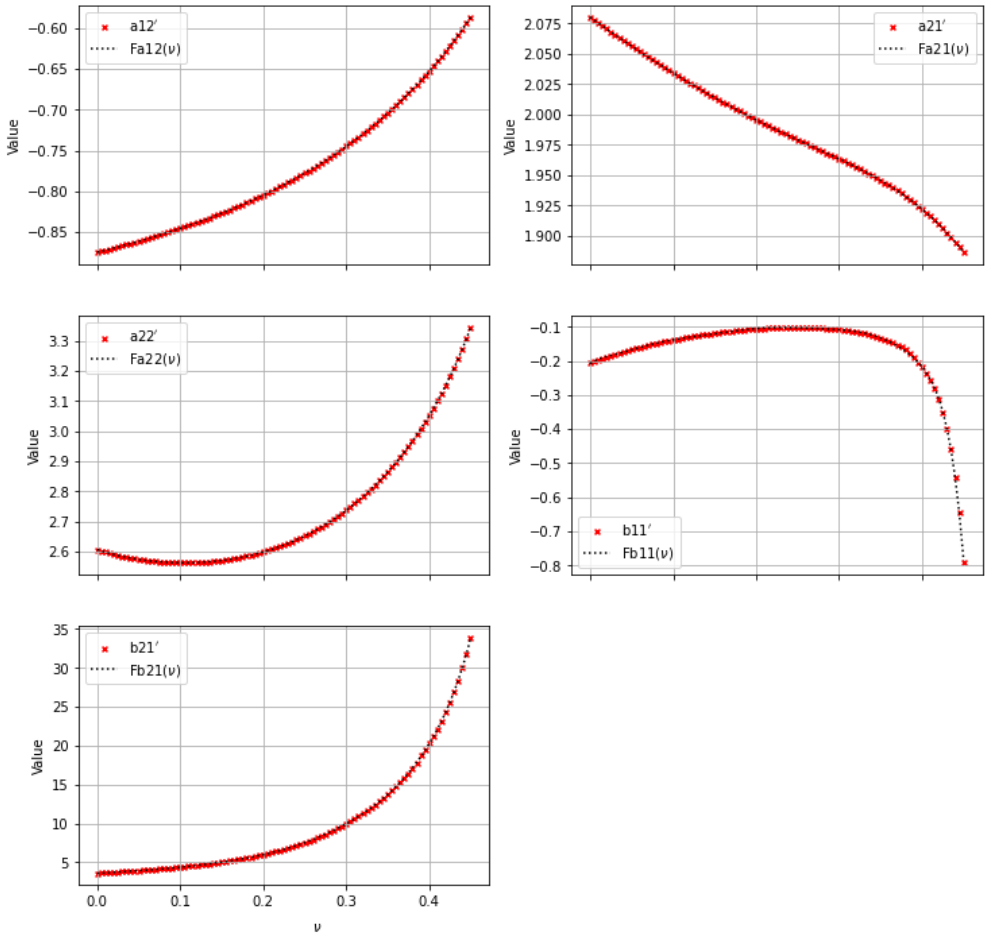

Figure A-8-1 The results of fitting $\mathbf{\Phi_{VanOpstal}}$ to $\mathbf{\Phi}$ $(term'\ )$ with red markers and the results of the $F_{term}(\nu)$ function as the black dotted line.

Table A-8-1 Table of constants for the term function. The term is in the column, and the order of the exponent is on the index. As an example, the constant $c_{a12,4} = -0.11434$.

coefficient / c	a_{12}	a_{21}	a_{22}	b_{11}	b_{21}
0	-0.87497	2.080217	2.607254	-0.20746	3.599964
1	0.24987	-0.49924	-0.93487	1.793036	0.29748
2	0.373257	0.364863	6.692275	-65.0529	412.1318
3	0.559165	1.290046	-26.9619	1811.649	-11373.6
4	-0.11434	-20.5632	137.5143	-27463.9	168274.2
5	5.814898	136.7318	-552.77	243211.9	-1431888
6	-16.207	-470.919	2339.165	-1321089	7450445
7	17.27946	1017.266	-7753.72	4458870	-2.4E+07
8	53.77717	-1753.25	16644.17	-9117099	46808093
9	-144.15	2168.227	-20383.6	10340718	-5.1E+07
10	104.9806	-1245.04	11179.3	-4994269	23350375

Table A-2 Results of the term function for specified Poisson's ratio's.

coefficient / Poisson's ratio	a_{12}	a_{21}	a_{22}	b_{11}	b_{21}
0.1	-0.84566	2.034158	2.563663	-0.13784	4.354947
0.15	-0.82697	2.013868	2.571187	-0.12007	5.009768
0.2	-0.80466	1.995513	2.599189	-0.10504	5.969443
0.25	-0.77774	1.979020	2.652585	-0.10281	7.521912
0.3	-0.74484	1.963281	2.738100	-0.10825	9.946381
0.35	-0.70402	1.945617	2.865399	-0.13224	13.71894

A.2 Comparing different solutions

In Figure A-2 the three different solutions for the $\mathbf{\Phi}$ function are shown. The $\mathbf{\Phi}$ solution is the function to be approximated. The $\mathbf{\Phi}_{VanOpstal}$ solution with the terms as determined by Van Opstal (1974). And the solution of $\mathbf{\Phi}_{VanOpstal}$ using the new terms: as determined by $F_{term}(\nu)$. Figure A2 also shows the Mean Squared Error (MSE), a measure on deviation to $\mathbf{\Phi}$.

Solutions at other Poisson's ratios and their deviation to $\mathbf{\Phi}$ are shown in Figure A-3.

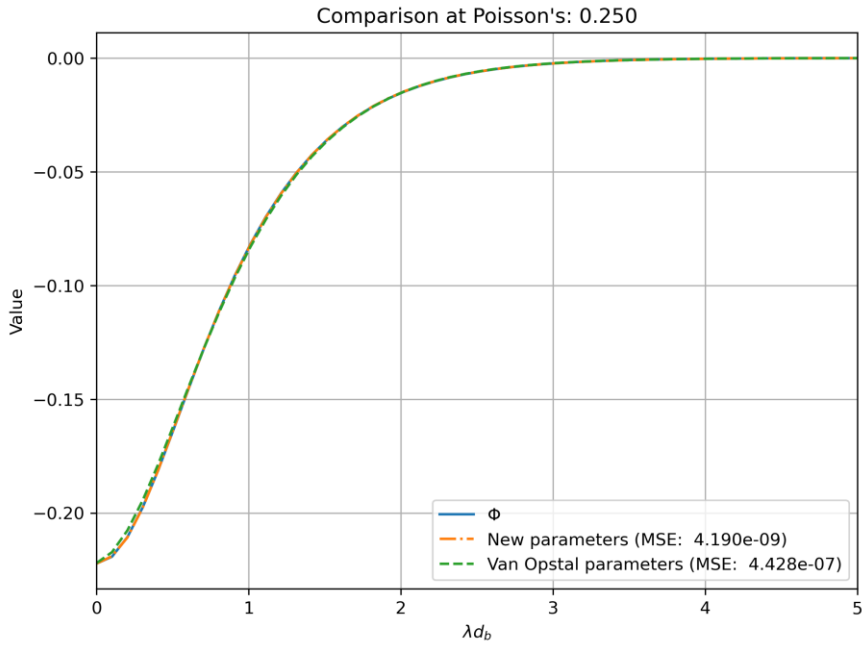

Figure A-2 Comparison between different solution of the $\mathbf{\Phi}$ function. The $\mathbf{\Phi}$ function (blue) is the function to be approximated and the other two lines have been constructed using $\mathbf{\Phi}_{VanOpstal}$. The green line represents the $\mathbf{\Phi}_{\mathrm{VanOpstal}}$ solution using the terms determined by him (1974) and the orange line the terms have been determined with $F_{term}(\nu)$.

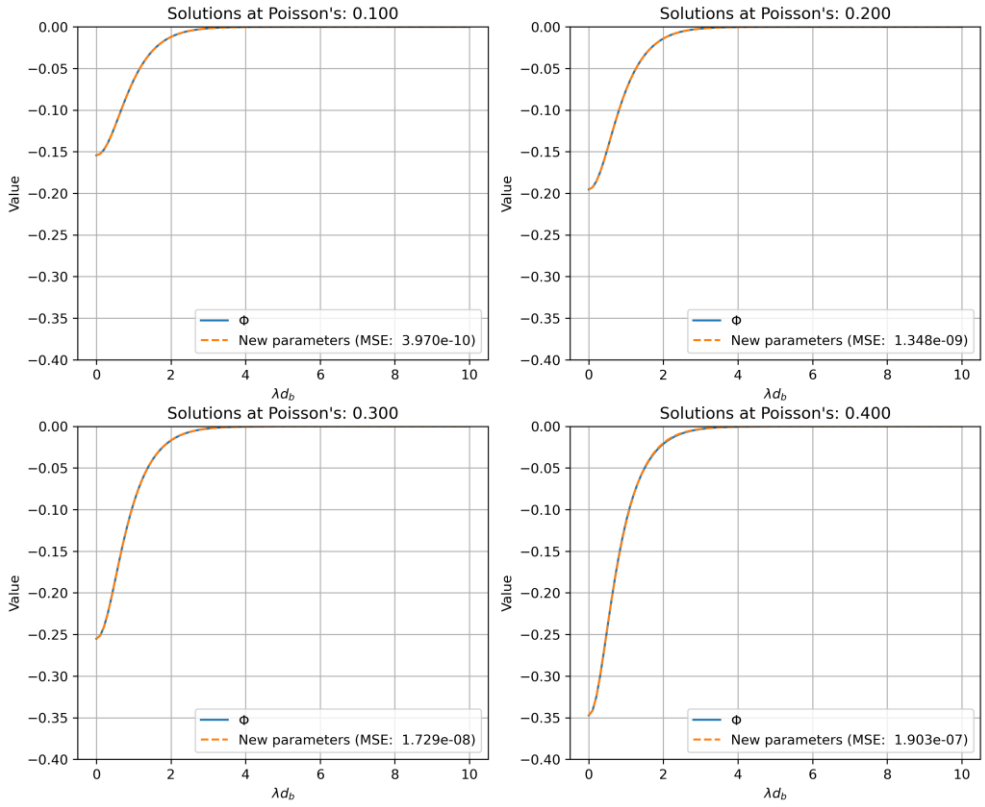

Figure A-3 Comparison between different solution of the **Φ** function. The **Φ** function (blue) is the function to be approximated and the orange line has been constructed using $\mathbf{\Phi}_{VanOpstal}$ and the terms as determined with $F_{term}(\nu)$.